AAPS PharmSciTech (2024) 25:21
https://doi.org/10.1208/s12249-024-02737-6

RESEARCH ARTICLE

Advancements in Amorphous Solid Dispersions to Improve Bioavailability

Screening of Organic Small Molecule Excipients on Ternary Solid Dispersions Based on Miscibility and Hydrogen Bonding Analysis: Experiments and Molecular Simulation

Sidian Zhang[1] · Huaqi Wang[1] · Xiuying Zhao[1] · Haiyan Xu[2] · Sizhu Wu[1]

Received: 12 September 2023 / Accepted: 27 December 2023 / Published online: 24 January 2024
© The Author(s), under exclusive licence to American Association of Pharmaceutical Scientists 2024

Abstract

The preparation of solid dispersions by mixing insoluble drugs with polymers is the main way to improve the aqueous solubility of drugs. The introduction of organic small molecule excipients into binary solid dispersions is expected to further enhance drug solubility by regulating intermolecular hydrogen bonding within the system at the microscopic level. In this study, we used carbamazepine (CBZ) as the target drug and polyvinylpyrrolidone as the solid dispersion matrix and screened the third component from 13 organic small molecules with good miscibility in the solid dispersion based on the principle of similarity of solubility parameters. The hydrogen bonding parameters and dissociation Gibbs free energy of the 13 organic small molecule-CBZ dimer were calculated by quantum mechanical simulation, and the tryptophan (Try) was identified as the optimal third component of organic small molecule. The migration of CBZ in binary and ternary systems was also analyzed by molecular dynamics simulation. On this theoretical basis, the corresponding solid dispersions were prepared, characterized, and tested for solubility analysis, which verified that the drug solubility was stronger for the system with the addition of polar fractions and the Try was indeed the best third component of organic small molecule compound, which was consistent with the simulation predictions. This screening method may provide theoretical guidance for drug modification design and clinical studies.

Keywords dissolution · intermolecular hydrogen bonding · molecular simulation · organic small molecule excipients · ternary solid dispersions

Introduction

Crystalline insoluble drugs make up more than 60% of all medications being researched at the moment [1]. It has become an urgent need to figure out how to increase these drugs' water solubility and bio-absorption so that they can be used more extensively. Researchers frequently use the addition of polymeric excipients to prepare solid dispersions to address the issue of the drugs' low solubility [2–5]. According to previous studies, most of the solid dispersions are used to disperse the drug by adding excipient substances that introduce hydrogen bonding between the drug and excipients. The addition of excipient makes while introducing specific polar groups in the solid dispersion, thus creating drug-excipient interaction. This allows the drug molecules to be stripped from their original crystallization and dispersed in the excipient matrix, thereby enhancing their solubility and bioabsorption properties [6, 7].

As a common non-covalent intermolecular interaction force, hydrogen bonding plays an important role in solid dispersion systems [8, 9]. On the one hand, most crystalline insoluble drugs have polar groups containing electronegative atoms in their molecular structure. The presence of these

✉ Haiyan Xu
xuhy@pumc.edu.cn

✉ Sizhu Wu
wusz@mail.buct.edu.cn

[1] State Key Laboratory of Organic-Inorganic Composites, Beijing University of Chemical Technology, Beijing 100029, People's Republic of China

[2] Institute of Basic Medical Sciences, Chinese Academy of Medical Sciences & Peking Union Medical College, Beijing 100005, People's Republic of China

groups induces the formation of hydrogen bonds between drug molecules, and drug molecules are oriented and arranged under such conditions to form long-range ordered crystal structures [10, 11]. On the other hand, the side groups or backbone structures of excipient materials also contain structures that could create intermolecular hydrogen bonds. These group structures can make hydrogen bonds with the drug molecule's donor or acceptor, creating the network that prevents the drug molecule from crystallization [12]. Thus, the core of improving drug solubility using solid dispersion technology lies in regulating the hydrogen bonds within the system, which means increasing the ratio of hydrogen bonds between drug-excipient as much as possible and reducing or replacing the hydrogen bonds between drug-drug molecules [6, 13].

Currently, some polymeric materials are commercially available, and many of these have been selected as polymeric excipients for the preparation of solid dispersion [14–16]. However, the single selection of commercially available polymeric excipients sometimes has certain drawbacks from the perspective of intermolecular hydrogen bond formation. For example, polyvinylpyrrolidone (PVP), a commonly used commercially polymeric excipient, has a ketone carbonyl group attached to its molecular structure that is a typical intermolecular hydrogen bonding proton acceptor [12, 17]. This structure can be effective for drugs with a high number of proton donors to form hydrogen bonding interactions. But, for drug molecules with a high proportion of proton receptor structures, PVP could not pass through to form effective hydrogen bonds with the active site of the drug. This instead exposed the proton acceptor of the drug and induced drug crystallization. Relevant studies have been conducted to demonstrate that there is still room for improving the solubility of solid dispersions formed by some drugs with PVP [18]. Therefore, based on the principle of hydrogen bonding, modification and adjustment are needed for such binary solid dispersion systems to further enhance the solubility performance of drugs.

It has been reported that the third component of some organic small molecule excipients can form a co-crystalline or amorphous state with the drug, which can produce certain improvement in the dissolution property of the drugs [19–21]. For example, Wu *et al*. investigated that controlling the molar ratio between carvedilol and organic acids allows the drug to form a co-amorphous system with organic small molecules [22]. Based on this clue, for the internal hydrogen bonding modulation of binary solid dispersions, this can be achieved by introducing organic small molecule excipients to form ternary solid dispersions, and the addition of these excipients theoretically enriches the internal hydrogen bonding network of the system and can form a synergistic effect with polymeric excipients. Fung and Suryanarayanan also prepared solid dispersions containing succinic acid and other solid dispersions based on PVP-ketoconazole (KTZ), respectively, to finally achieve a 30 ~ 80% increase in dissolution rate [23]. By this way, there is a synergistic effect for the improvement of properties such as solubilization effect of insoluble drugs. However, many types and numbers of organic small molecule excipients may be considered as the third component candidates, including various organic acids [24], amino acids [25], and sugars [26]. For these excipients, the screening mechanism for specific drugs is still not clear, especially at the molecular level. In addition, there is a lack of quantitatively analysis of the microscopic formation and synergistic effects of ternary solid dispersion systems compared with binary solid dispersion systems [27].

With the development of computer technology, multi-scale simulations such as quantum mechanical simulations and molecular dynamics simulations can explain the internal formation mechanism and performance advantages of solid dispersions [28–33]. For example, Paroma Chakravarty *et al*. calculated the difference in solubility parameter (δ) between GENE-A and HPMCAS by means of molecular dynamics simulations to provide a criterion for the miscibility of solid dispersions [34]. Li Bin *et al*. used quantum mechanical simulations to construct a model of an associative dimer consisting of two drug molecule units of toltrazuril and patrozuril and quantitatively analyzed the intermolecular hydrogen-bonding interactions while also obtaining the binding site with the lowest energy [35]. It can be seen that the simulation method is of advantage for the analysis of micro-mechanisms such as molecular migration and diffusion, system miscibility [36], and intermolecular forces. In addition, compared with the characterization of interactions, multi-scale simulation can quantify the strength of intermolecular interactions, mainly hydrogen bonding, which can solve the shortcomings of experimental methods that make it deeply probe the binding mechanism at the molecular level.

In this study, an antiepileptic drug carbamazepine, with the molecular structure shown in Fig. 1, was selected as the model drug [37]. Among them, the amide group attached to the drug is considered as the active site for the formation of hydrogen bonds, containing both donor and acceptor. The research is proposed to obtain the solubility parameters based on molecular dynamics simulation and analyze the thermodynamic parameters of hydrogen bond dissociation based on quantum mechanical simulation (QM) method, with a view to screening out the optimal third component molecular structure. On the basis of the determining third component, molecular dynamics (MD) simulation was used to quantitatively calculate the binding energy of the system, hydrogen bonding concentration, and other microscopic parameters and to study the variation rule of drug molecules' migration resistance in binary and ternary solid dispersions.

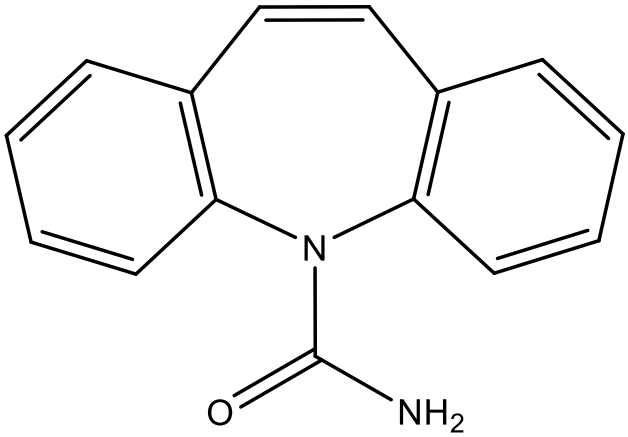

Fig. 1 Molecular structure of carbamazepine (CBZ)

Then, the simulation results were verified by relevant experimental characterization and performance tests to explore the theoretical mechanism of the third component incorporation.

Molecular Simulation Methodology

Both quantum mechanical (QM) and molecular dynamic (MD) simulations were used in this study as methods of simulation. The software used is Materials Studios developed by Accelrys, USA. Among them, the optimal third component screening is determined by QM and MD methods, and the solid dispersion system performance prediction and comparison is realized by MD simulation method.

Details of Quantum Mechanical Simulation

QM simulations were run and calculated through the part of Dmol^3 in the software. The main parameters obtained through QM simulations include the conformation, geometric parameters, dissociation Gibbs free energy, and other thermodynamic parameters of the dimer model involving organic small molecules in association with the drug molecule. All these parameters are the key parameters to characterize the molecular interaction and can be used as an important basis for third component screening. The energy minimum conformation of the model is first obtained using the Geometry Optimizer command in the Forcite module. Based on this, computations were made using Dmol^3's part of geometric optimization. According to density generalization theory (DFT) [38], the total molecular energy is expressed as a generalization of the density function of electrons, and the ground state properties of the multi-electron system can be determined accordingly. The generalized gradient approximation (GGA) in the form of Perdew-Burke-Ernzerhof (PBE) is used to approximate the

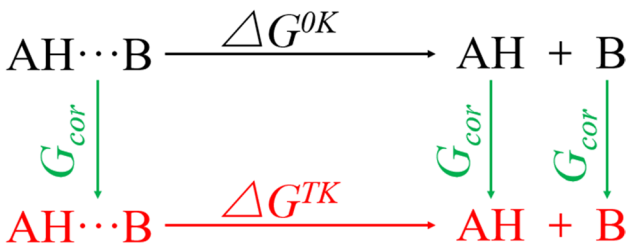

Fig. 2 Schematic diagram of the thermodynamic cycle of dissociation of hydrogen bonded dimer and calculation of dissociation energy

exchange–correlation potential in the KS equation. The wave function of the system is described by the TNP unit [39, 40].

The thermodynamic cycle and energy calculation of the hydrogen bond dissociation reaction can be simplified as Fig. 2. In this figure, A and B are both strongly electronegative atoms (N/O/F), while H, which is connected to A, is electron-deficient hydrogen. Therefore, AH and B are the proton donor and the proton acceptor of the intermolecular hydrogen bond, respectively [41].

Besides, according to the thermodynamic cycle diagram of hydrogen bond dissociation in Fig. 2, the Gibbs free energy of dimer dissociation at a specific temperature T can be calculated from Eq. (1) [41].

$$\Delta G^{\theta,T} = \left(G^{T}_{\mathrm{cor}}(AH) + G^{0K}(AH)\right) + \left(G^{T}_{\mathrm{cor}}(B) + G^{0K}(B)\right) - \left(G^{T}_{\mathrm{cor}}(AH\cdots B) + G^{0K}(AH\cdots B)\right) \quad (1)$$

In the formulation above, $G^{0\mathrm{K}}$ represents the standard Gibbs free energy of AH, B, $AH\ldots B$ at 0 K, and $G^{\theta,\,T}$ refers to the standard Gibbs free energy of AH, B, $AH\ldots B$ at T K, respectively. Both free energies, G_{cor} (with cor subscript) refers to the Gibbs free energy corrected value of AH, B, and $AH\ldots B$ calculated from 0 K to T K.

Details of Molecular Dynamic Simulation

The calculation of the solubility parameters of the organic small molecules and the comparison of the performance differences between binary and ternary composite systems were achieved by means of molecular dynamics simulations. First, under COMPASS II force field [31], periodic unit cell models of single and composite systems are executed under Forcite module with geometry optimization procedure to obtain the cell with the lowest energy. On this basis, 200 cycles of annealing process were executed at a time, with temperatures ranging from 300 to 500 K. The kinetic process was selected as a regular system synthesis (NVT) and a constant temperature and pressure system (NPT), running for 500 ps and 1000 ps, respectively. The energy of the system is monitored during the calculation, and the system is

considered to be converged when the fluctuation range is less than 10% [42].

Theoretical Results and Discussion

Screening Process for Organic Small Molecule Excipients

Through relevant literature research [23, 43, 44], 13 organic small molecules were selected that usually be used as modulators of intermolecular interactions in drug-polymer systems. The molecular formulae and their IDs in this study are shown in Fig. 3.

The preliminary screening of the 13 organic small molecules to be candidate was carried out using the principle of "similar miscibility of solubility parameters" [45]. The solubility parameter is defined as the square root of the cohesive energy density (CED) of a substance and has important applications in the field of evaluating the miscibility of components of a system [46].

In solid dispersions and pharmacological studies, two components are usually considered compatible when the absolute value of the difference between their solubility parameters is less than 7 $(J/cm^3)^{1/2}$, and vice versa. The results of the solubility parameter values for 13 organic small molecules and their absolute values of solubility parameter differences with CBZ, respectively, are shown in Fig. 4. It can be found that the solubility parameters of 2, 8, 9, 10, 11, and 13 are less than 7 $(J/cm^3)^{1/2}$ from the solubility parameter of carbamazepine [34]. Therefore, these six organic small molecule additives were initially screened out for subsequent calculations.

Based on the screening of six organic small molecules, the molecular model of the lowest energy CBZ-small molecule-conjugated dimer was constructed, and these conformations and hydrogen bonding morphology are shown in Fig. 5. From the conformational information, it can be found that only a single hydrogen bond is formed between 10, 11, and CBZ, while two hydrogen bonds are formed between CBZ and 2, 8, 9, and 13 small molecules, which indicates that CBZ can act as both a donor and an acceptor in the process of forming hydrogen bonding interaction with the above molecules. The *L* represents the bond length of the hydrogen bond and *A* refers to the bond angle of the hydrogen bond in Fig. 5. For intermolecular hydrogen bonds, it is usually considered that the smaller the bond length and the larger the bond angle, the higher the strength will be [47]. It can be found that the intermolecular hydrogen bonds between the two conjoined dimer models of CBZ-10 and CBZ-11 are significantly weaker than the remaining four dimers. Therefore, four organic small molecules, 2, 8, 9, and 13 in this step, were continued to be screened on the results of the analysis of the hydrogen bond conformation for the follow-up study.

For the above four hydrogen bonded dimer of CBZ-2, CBZ-8, CBZ-9, and CBZ-13, the Gibbs free energy (ΔG) of

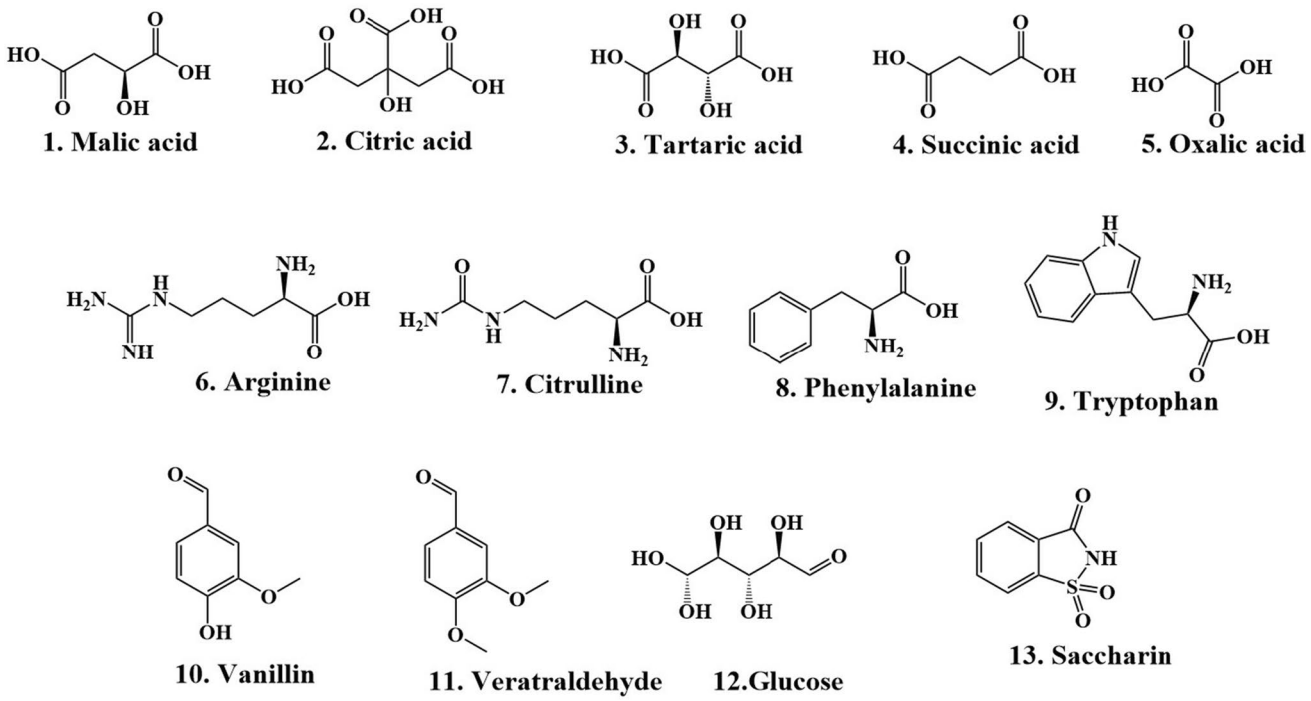

Fig. 3 Structures of 13 organic small molecule excipients to be candidates for incorporation into binary solid dispersion systems and their IDs

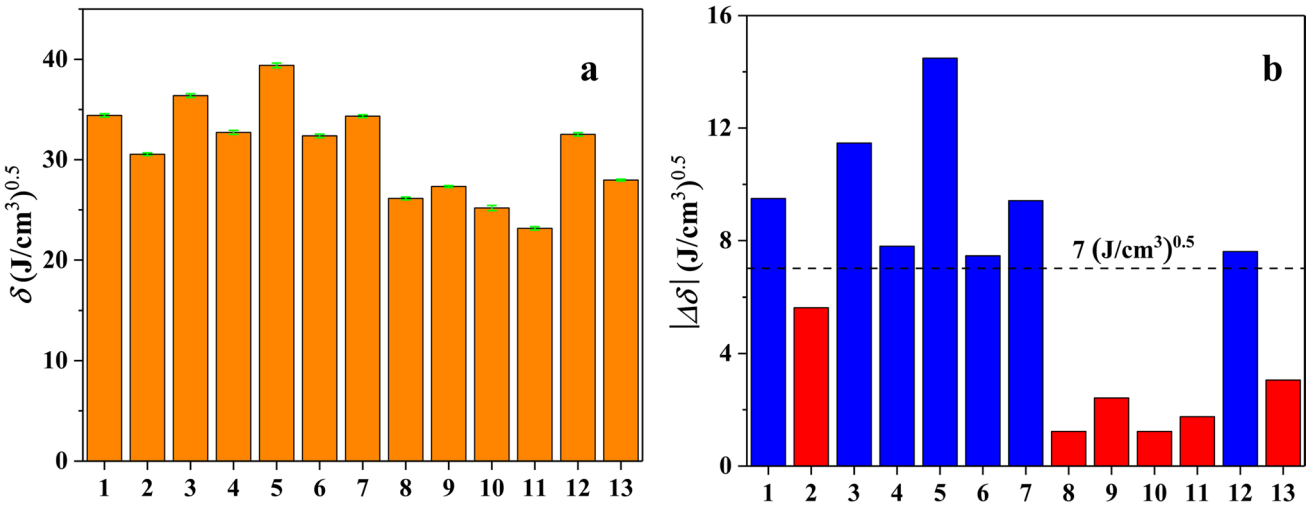

Fig. 4 **a** Values of solubility parameters of 13 organic small molecules. **b** Absolute values of the difference between solubility parameters of each small molecule and CBZ (with the screened six small molecule candidates in red)

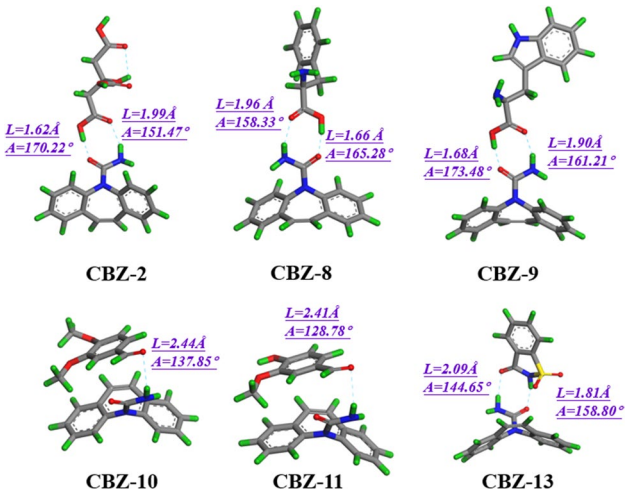

Fig. 5 Three-dimensional spatial conformation and geometrical parameters of the conjugated dimer of CBZ with 2, 8, 9, 10, 11, and 13 organic small molecules

the dissociation reaction was calculated separately according to Eq. (1) in the "Details of Quantum Mechanical Simulation" section. The results are shown in Fig. 6a, and the dissociation Gibbs free energies are CBZ-9, CBZ-13, CBZ-2, and CBZ-8 in descending order, and the corresponding small molecules are tryptophan, citric acid, saccharin, and phenylalanine in descending order. Therefore, it can be assumed that the intermolecular hydrogen bonding formed between the organic small molecule tryptophan (No. 9) and CBZ is the strongest among these four systems.

Besides, for the dissociation reaction equilibrium constant $\ln K^{\theta}$ was equally examined. The calculation procedure is shown in Eq. (2) [48].

$$ln\ K^{\theta} = ln\frac{c(AH)\cdot c(B)}{c(AH\cdots B)} = -\frac{\Delta G^{\theta}}{RT} \tag{2}$$

where R represents the ideal gas constant, T is the reaction temperature, and $c(AH)$, $c(B)$, and $c(AH\cdots B)$ are the moles of proton acceptor, proton donor, and associative dimer concentration, respectively. The standard Gibbs free energy ΔG^{θ} is obtained from Eq. (1).

From the calculated equations, it can be inferred that this parameter is related to the hydrogen bond concentration. When the concentrations of the donor and acceptor units composing the conjugated dimer are constant, the lower the value of $\ln K^{\theta}$, the higher the molar concentration of the constituent hydrogen bonds. It can be inferred from Fig. 6b that the hydrogen bond concentration in the four systems composed of CBZ is tryptophan > saccharin > citric acid > phenylalanine from the highest to the lowest. Therefore, the No. 9 organic small molecule, also known as tryptophan, was once more confirmed as a suitable third component to be added to the CBZ solid dispersion.

Performance Prediction and Analysis of Designed Excipient

As shown in Fig. 7, the binary complex system model of CBZ/PVP and the ternary complex model of CBZ/PVP/Try were constructed on the basis of determining the selection of tryptophan (Try) as the third small molecule component as the research object. In the systems above, the molecular chains of PVP contained 50 repeating units. Among them, the mass ratio of CBZ to polymer was 1:9 according to the ratios of solid dispersions prepared by previous researchers [23], while the third small molecule components were

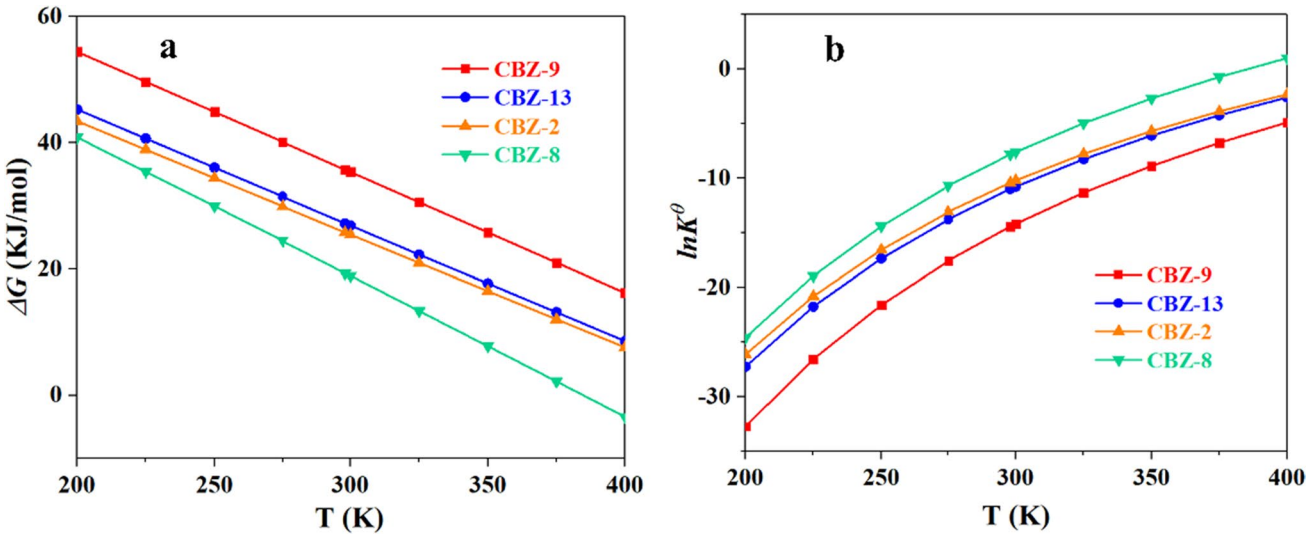

Fig. 6 **a** Gibbs free energies (ΔG) for hydrogen bond dissociation processes in the range of 200–400 K for the four conjoined dimers. **b** Logarithm of equilibrium constants ($\ln K^{\theta}$) for dissociation processes in the same temperature range

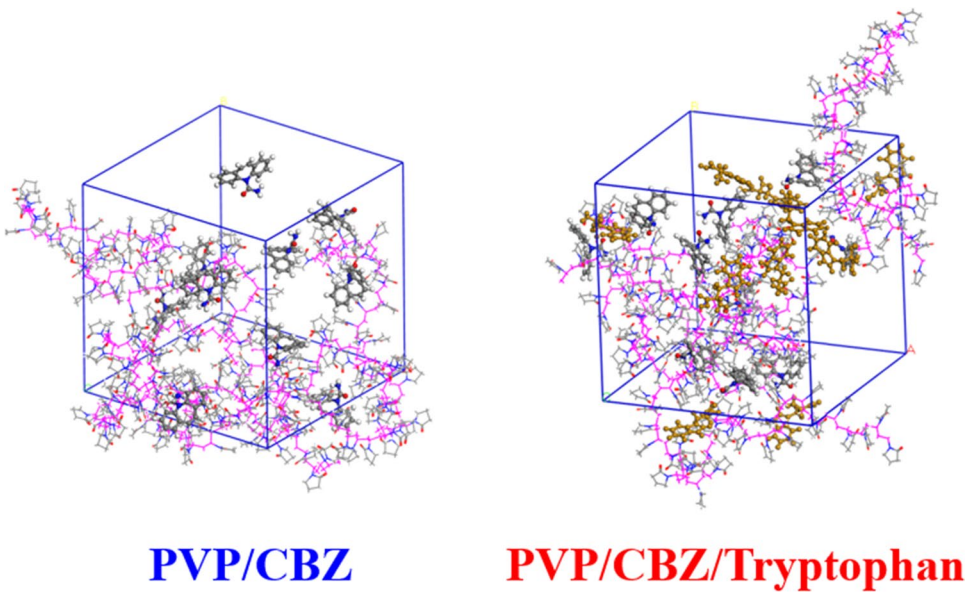

Fig. 7 Periodic unit cell model of CBZ/PVP binary composite system and CBZ/PVP/Try ternary system, where the gray part is carbon atoms, the red part is oxygen atoms, the blue part is nitrogen atoms, the white part is hydrogen atoms, the molecular chain backbone structure of the polymer is magenta, and the Try molecule is marked by orange

kept in equimolar ratio with CBZ. Therefore, the number of molecules of CBZ, PVP, and Try in the periodic repetitive cell model is set as 10, 4, and 10, respectively.

Dispersibility of CBZ Molecules

The degree of dispersion of drug molecules in the matrix has an important influence on the property transformation of solid dispersions. Firstly, the migration resistance of small molecules in the system was investigated using the mean square displacement *MSD*, which represents the mean value of the squared displacement of the object of study at a specific time, and is an important indicator of molecular migration and diffusion. *MSD* is calculated as shown in Eq. (3) [46].

$$MSD = \frac{1}{N}\sum_{i=1}^{N}\left[r_i(t) - r_i(0)\right]^2 \tag{3}$$

In Eq. (3), N represents the number of particles counted, and $r_i(0)$ and $r_i(t)$ denote the position coordinates of particles at moment 0 and moment t, respectively.

The variation of *MSD* of CBZ drug molecules in both systems is shown in Fig. 8a. It can be demonstrated that

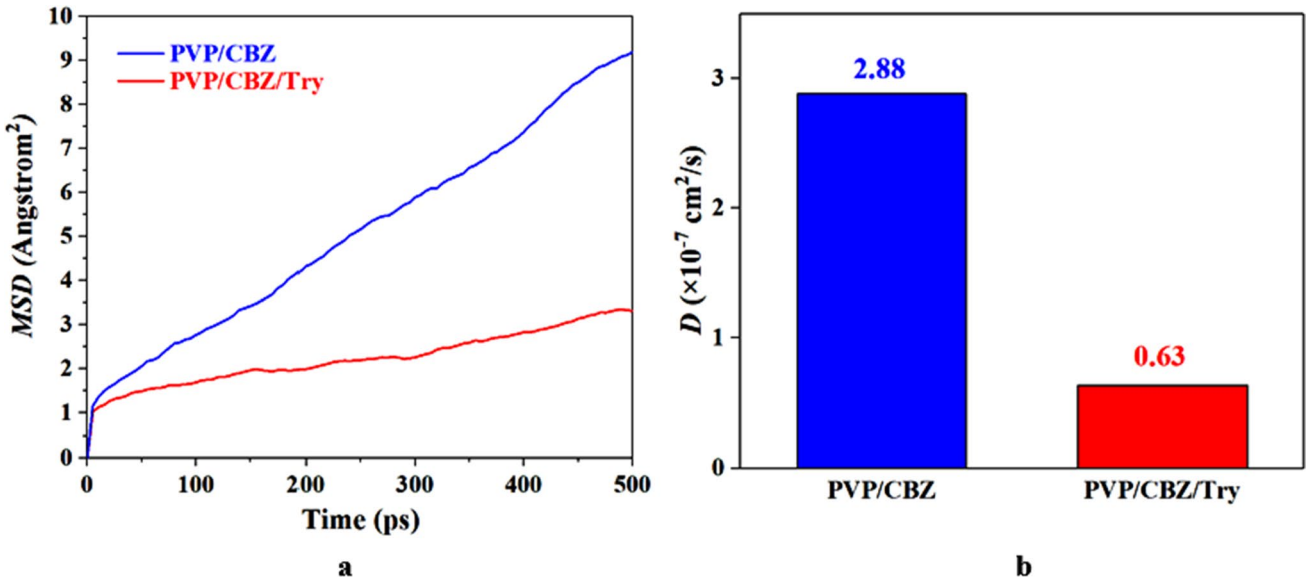

Fig. 8 **a** *MSD* curves of drug small molecules in 0–500 ps; **b** diffusion coefficients (*D*) of CBZ molecules in two systems

the *MSD* of CBZ molecules is lower in the ternary system containing organic small molecule Try, which means that the CBZ molecules in the CBZ/PVP/Try ternary system are more resistant to migration than the CBZ molecules in CBZ/PVP binary system.

To further quantify the migration and diffusion of drug molecules, the diffusion coefficient (*D*) of CBZ molecules was extracted from the MSD results. The diffusion coefficient (*D*) of a molecule is calculated by the Einstein equation, as shown in Eq. 4 [46].

$$D = \lim_{t\to\infty} \frac{\left\{ \left[r_i(t) - r_i(0) \right]^2 \right\}}{6t} = \frac{MSD}{6t} \tag{4}$$

The differential part of Eq. (4) can be approximated as the derivative of *MSD* to time *t*, that is, the slope value of the *MSD* curve. The diffusion coefficient results were quantified as in Fig. 7b. In the CBZ/PVP/Try ternary system (red), the *D* value of CBZ was reduced by 78% compared to the binary system (blue), which further indicates that the addition of organic small molecule Try can inhibit the migration and diffusion of CBZ molecules in the spatial range.

At the same time, the binding energy (E_{binding}) is used to examine the binding effect of CBZ components with carrier components and indirectly reflects the degree of dispersion of CBZ and the inhibition of drug crystallization by excipients. The calculation procedure of E_{bingding} is shown in Eq. (5) [28].

$$E_{\text{binding}} = -\left(E_{\text{total}} - E_{\text{CBZ}} - E_{\text{carrier}}\right) \tag{5}$$

In Eq. (5), E_{total} indicates the total energy of the system, E_{CBZ} is the total energy of carbamazepine, and E_{carrier} indicates the total energy of the remaining excipients in the system, except CBZ.

The results are shown in Fig. 9. It can be found that the binding energy of CBZ and excipients in the ternary system with the addition of Try increased by 18.8% compared with the binary system. On the one hand, the binding effect of CBZ with the excipients in the system with the addition of the third component is stronger than that in the binary system. On the other hand, it can be speculated that CBZ will present better dispersion in the ternary system.

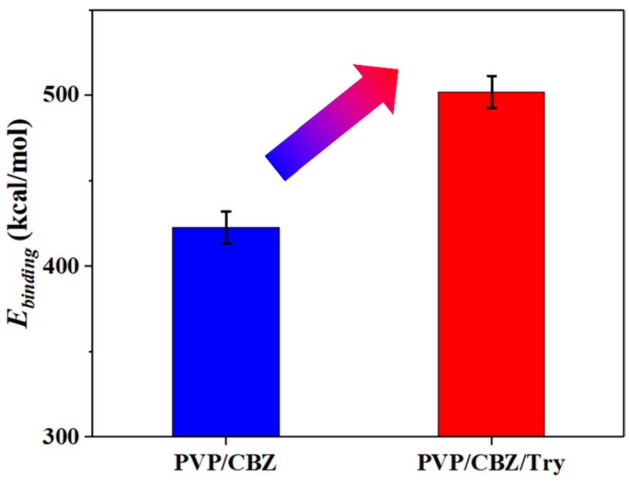

Fig. 9 The binding energy (E_{binding}) between CBZ and the excipient in both systems

Intermolecular Interaction Discussion

Based on the characteristics of the CBZ molecule and the accompanying polar groups, the potential proton donors and proton acceptors within the molecule were identified and labeled as shown in Fig. 10a. The proton donor grouping of Type A hydrogen bonds is the amino hydrogen within the carbamazepine molecule, and the proton acceptor grouping includes all the N and O electronegative atoms in the PVP and Try molecules. Similarly, Type B hydrogen bonds have the O atoms in the carbamazepine molecule as the proton acceptor grouping, and the proton donor grouping is all the electron-deficient hydrogens in the Try molecule that are bonded to electronegative atoms. The radial distribution function (*RDF*, $G(r)$) is defined as the probability distribution of finding an atom at a distance r from another atom and can be used to monitor the type of hydrogen bonding within the system [49]. When r is monitored in the range of 2–2.5 Å for significant peak patterns, it can be assumed that some type of intermolecular hydrogen bonding is present in the system, which is beneficial for the improved dispersion [45].

Based on the results in Fig. 10b as well as Fig. 10c, it is known that only type A hydrogen bonding exists in the CBZ/PVP binary system, i.e., CBZ can only act as a proton donor in this system. In contrast, in the CBZ/PVP/Try ternary system, both type A and type B hydrogen bonds are present, which indicates that the addition of Try plays a strong role in regulating the nets of intermolecular hydrogen bonds in the system.

For the type A and type B hydrogen bonds involved in both systems, the molar concentrations of hydrogen bonds

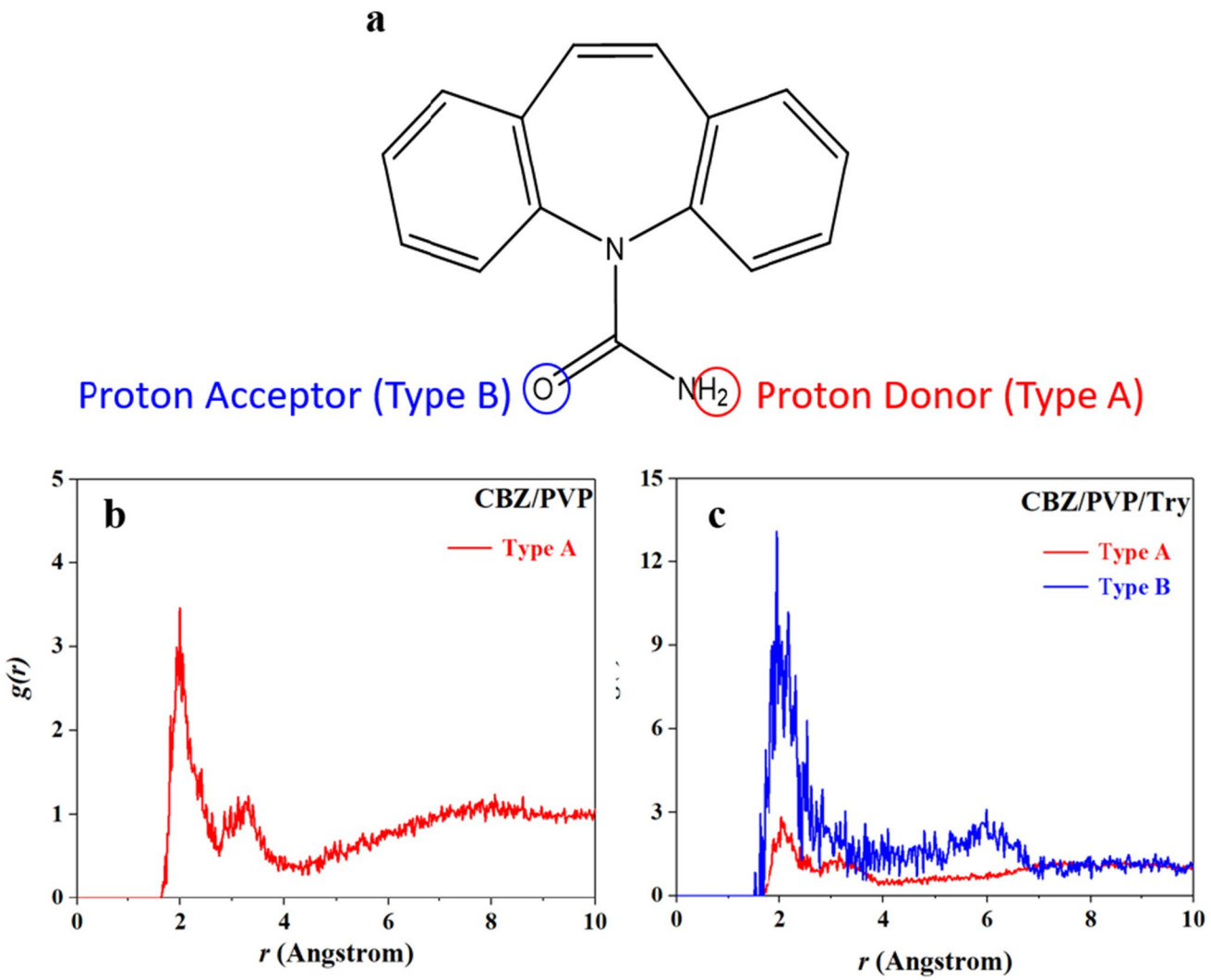

Fig. 10 **a** Typification of hydrogen bonding proton donors and acceptors within CBZ molecules; **b** radial distribution function of intermolecular hydrogen bonding within the CBZ/PVP binary system; **c** radial distribution function of intermolecular hydrogen bonding within the CBZ/PVP/Try ternary system

(C_{HBs}) were used to quantify their contents [50]. The calculation procedure for this parameter is shown in Eq. 6.

$$C_{HBs} = \frac{N_{HBs}/N_A}{V} \quad (6)$$

In Eq. (6), N_{HBs} is the statistical number of hydrogen bonds, V is the volume of the unit cell, and N_A is Avogadro's constant. The concentrations of type A and type B hydrogen bonds in both systems were quantitatively accounted for, as shown in Fig. 11. From the results, it can be seen that the intermolecular hydrogen bonding in the ternary CBZ/PVP/Try system not only has more B-type hydrogen bonding than that in the CBZ/PVP system, but also has a relatively higher overall intermolecular hydrogen bonding concentration. This suggests that the hydrogen bonding between the CBZ and the excipient inside the ternary system is also stronger.

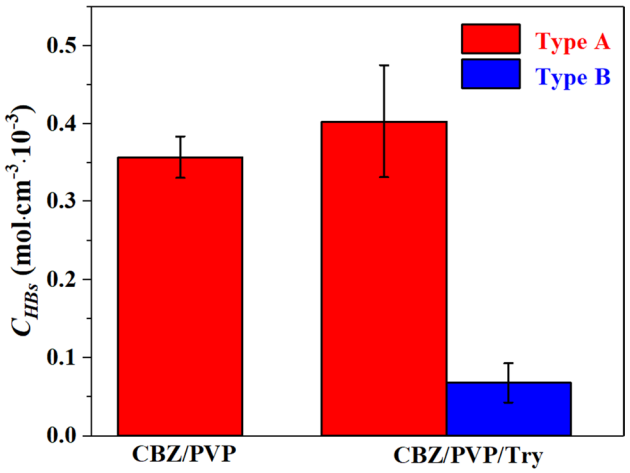

Fig. 11 Intermolecular hydrogen bonding concentrations (C_{HBs}) within CBZ/PVP and CBZ/PVP/Try systems

The mechanisms of solid dispersion formation for the two systems inferred from the results of the simulations are illustrated in Fig. 12. In the CBZ/PVP system, CBZ binds to the PVP molecular chain with the help of type A hydrogen bonding as a proton donor for hydrogen bond formation and PVP as a proton acceptor. The polymer, however, is unable to bind to the ketone carbonyl group of carbamazepine due to the lack of sites that act as proton donors, which induces the formation of more drug-drug hydrogen bonds. Meanwhile, in the CBZ/PVP/Try ternary system, the addition of organic small molecule Try not only elevates the concentration of type A hydrogen bonds in the system but also introduces type B hydrogen bonds to bind with CBZ, which plays a role in inhibiting migration and destroying crystallization. Besides, these effects above are expected to improve the dispersion state and enhance the dissolution performance of solid dispersions.

Materials and Methods

Materials

Carbamazepine (CBZ) was obtained from Jiuding Chemical Co., Ltd., Shanghai, China. Polyvinylpyrrolidone (PVP) was purchased from Solarbio Co., Ltd., Beijing, China, and the number average molecular weight of PVP is 2.0×10^4. L-tryptophan (Try) was achieved from Macklin Co., Ltd., Beijing, China. The anhydrous ethanol and deionized water involved in the preparation process are industrial grade solvents. The above-mentioned raw materials are directly put to use without further research.

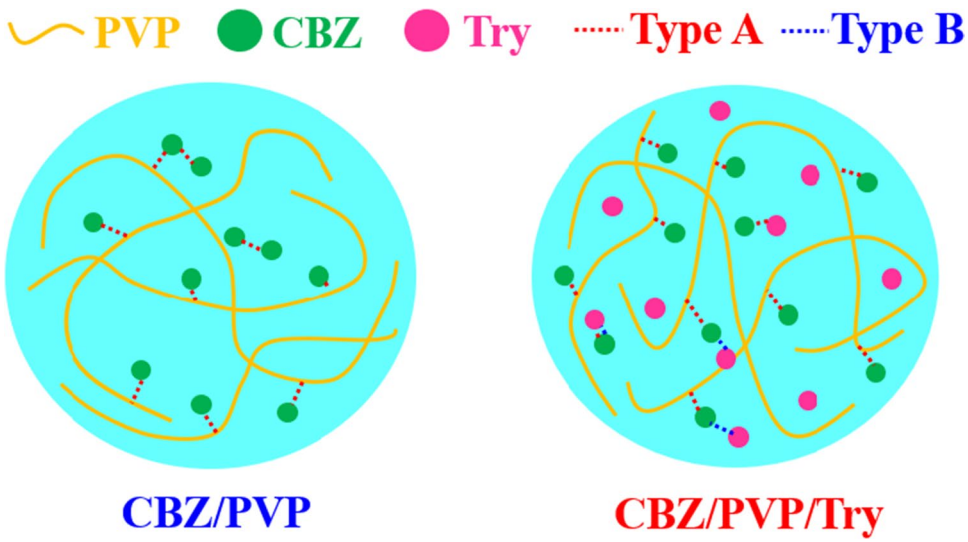

Fig. 12 Schematic diagram of the intermolecular hydrogen bonding mechanism between binary and ternary solid dispersions of CBZ

Preparation of Two Solid Dispersions

The solid dispersion samples for this study were prepared by the solvent-lyophilization method. For the binary solid dispersions and the simulation mixing ratio (The mass ratio of CBZ to PVP is 1:9), 2.70 g of PVP powder, 0.30 g of CBZ powder were firstly weighed, and 150 ml of anhydrous ethanol was added, and the mixture was magnetically stirred for 1 h to dissolve fully. On this basis, the CBZ/PVP-ethanol solution was rotary evaporated at 35°C until a large amount of organic solvent was removed to obtain the CBZ/PVP concentrated product. The concentrated product was transferred to a freeze dryer for 24 h and then ball milled and passed through 80 mesh sieve to finally obtain a binary solid dispersion powder of CBZ/PVP. This obtained solid dispersion sample was labeled as CBZ/PVP-SD.

For the ternary solid dispersion, an additional 0.26 g of Try was added at the time of weighing to maintain an equimolar amount with CBZ, and about 15 ml of deionized water was added during the dissolution process to ensure the full dissolution of Try. Other than that, the rest of the operation was consistent with the preparation of binary solid dispersions. The solid dispersion obtained from the final product was labeled as CBZ/PVP/Try-SD.

Measurements and Characterization

X-Ray Diffractometry (XRD)

The *X-ray* diffractometer (XRD-600, Shimadzu, Japan) was used to qualitatively detect the crystallinity of the samples. XRD tests were performed on an XRD-600 diffractometer with a Cu Kα radiation source. The 2θ range of the test is from 5 to 60°.

Differential Scanning Calorimetry (DSC)

Differential scanning calorimetry (Mettler DSC3, Mettler, Switzerland) is applied to characterize the thermal behavior of a sample such as melting, crystallization, and glass transition. The temperature of the test is monitored starting from 0°C, with a temperature rise of 10°C per minute and a monitoring end point of 220°C. The gas atmosphere is nitrogen. The flow rate of nitrogen for DSC was in the range of 250–300 mL/min.

Scanning Electron Microscope (SEM)

Scanning electron microscope was used to monitor the surface morphology of the samples. CBZ drug and solid dispersion samples were monitored by scanning electron microscope (SU8010, Hitachi, Japan). Samples were pretreated by applying on conductive adhesive and sprayed with gold.

Fourier Infrared Spectroscopy (FT-IR)

FT-IR spectroscopy (Vertex 70v, Bruker, Germany) is utilized to monitor changes in sample moieties and intermolecular interactions. As both drug and solid dispersions were powdered samples, the spectroscopy was performed using the potassium bromide compression method for the wavenumber range of 4000–400 cm^{-1}. This infrared spectrometer has a resolution of 4 cm^{-1}.

Dissolution Tests

UV–Vis Spectrophotometry The test of UV–Vis absorption is designed to determine the wavelength of maximum absorption of carbamazepine in solution. Five CBZ-ethanol solution samples were configure according to a certain concentration gradient, and the UV–Vis spectrophotometric curves were measured in the wavelength range of 400–200 nm using a UV spectrophotometer (UV-2600, Shimadzu, Japan). The highest absorbance in this range was monitored, and the standard solubility curves were plotted sequentially.

Dissolution Test The dissolution test reflects the change in concentration of drug released from solid dispersions with time and is an important indicator of sample solubility. Dissolution testing is done by an automatic dissolution meter (FOCS, China). The dissolution medium was a hydrochloric acid solution with pH = 1.2 simulating the gastric fluid environment, the dissolution temperature was set at 37.0 ± 0.5 ℃, the dissolution method was paddle method, and the stirring speed was 100 rpm. A mass of 20 mg of pure drug CBZ and two solid dispersion samples containing 20 mg active ingredient of CBZ were weighed and immersed in the dissolution medium. Samples were taken at 5 min, 10 min, 15 min, 30 min, 60 min, 90 min, 120 min, and 180 min to identify the UV–Vis absorbance and then to determine the CBZ content in the medium.

Experimental Results and Analysis

Results and Analysis of XRD

The diffraction patterns of CBZ with its solid dispersion are shown in Fig. 13. Among them, the diffraction spectrum of pure CBZ has dense crystalline diffraction peaks in the range of 2θ for 0–60°, which can be inferred that CBZ is a crystalline sample. On the contrary the samples of CBZ/PVP-SD and CBZ/PVP/Try-SD show amorphous diffraction peaks in this range. It can be concluded that the solid dispersions

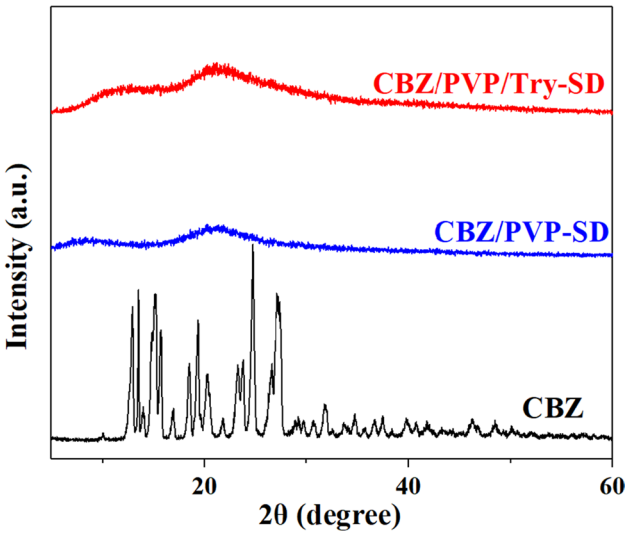

Fig. 13 XRD diffraction patterns of CBZ, CBZ/PVP-SD, and CBZ/PVP/Try-SD

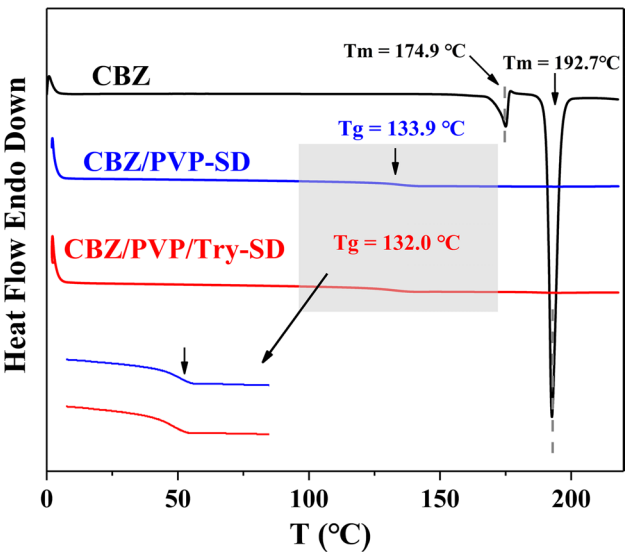

Fig. 14 DSC curves of CBZ, CBZ/PVP-SD, and CBZ/PVP/Try-SD

modified with the addition of excipients are more dispersed with the drug relative to the original CBZ, having the crystalline state transformed to the amorphous state.

Results and Analysis of DSC

The DSC curves of the samples are shown in Fig. 14. Among them, the CBZ crystals contain two forms, which are type I and type III [51]. It corresponds to two sharp melt heat absorption peaks at the temperatures 174.9°C and 192.7°C, respectively. And the DSC spectra of both solid dispersion samples disappeared the characteristic melting peaks at these two temperatures. Besides, the glass transition temperatures (T_g) of CBZ/PVP-SD and CBZ/PVP/Try-SD were 133.9°C and 132.0°C, respectively. On the one hand, the T_g obtained for CBZ and L-Try were 42°C (the temperature in this literature is in Kelvin, 315 K) and 141°C [52, 53], respectively. In contrast, the T_g of CBZ/PVP-SD and CBZ/PVP/Try-SD measured in this study were 133.9°C and 132.0°C, respectively, which were significantly higher than that of CBZ. It suggests that the physical stability of the solid dispersion is higher than that of the pure drug sample. On the other hand, according to the rule of thumb that amorphous solid dispersions should be stored below the temperature of "*Tg*-50°C" [51], it means both prepared solid dispersions can be stored for a long time under conventional conditions.

Surface Structure Observation

For the surface morphology of CBZ and the corresponding binary and ternary solid dispersions, observations were made using the scanning electron microscopy method, and the results are shown in Fig. 15. It can be seen that many of the scanning electron microscopy images of the CBZ powder particles are angular particles with a characteristic and significant crystalline structure. On the contrary, CBZ/PVP-SD and CBZ/PVP/Try-SD showed irregular and smooth particles in the microscopic morphology, as the surface morphology in the amorphous state.

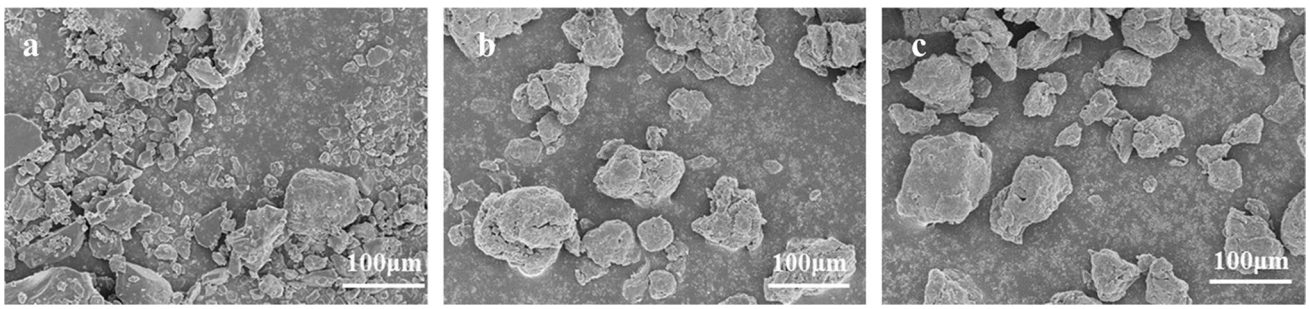

Fig. 15 Scanning electron micrographs of three samples: **a** CBZ; **b** CBZ/PVP-SD; **c** CBZ/PVP/Try-SD

Results and Analysis of FT-IR

The FT-IR spectra of CBZ, PVP, Try, and two solid dispersions are shown in Fig. 16. For CBZ, its N–H stretching characteristic peak of primary amine was present at the wavenumber of 3462 cm^{-1}. The stretching vibrational peak of C = O was present at 1678 cm^{-1} as well as the deformation characteristic peak of N–H at 1602 cm^{-1}. And the carbonyl stretching vibration peak on the molecular chain is present at 1715 cm^{-1} for PVP. According to the characteristics of CBZ/PVP-SD and CBZ/PVP/Try-SD spectra, the C = O characteristic peak position of PVP was significantly blue-shifted, which indicated that the carbonyl group of PVP was involved in the formation of intermolecular hydrogen bonds with CBZ and acted as a proton acceptor. Meanwhile, the N–H stretching vibration peak of CBZ disappeared in both solid dispersions, which is also an evidence that the amino group of CBZ is involved in the formation of intermolecular hydrogen bonds and acts as a proton donor. This evidence demonstrates the formation of Type A hydrogen bonds between CBZ and PVP in the solid dispersion as discussed in the molecular simulation above.

In addition, the amino stretching vibration peak of Try (3407 cm^{-1}) and the hydroxyl absorption band carried by the carboxyl group (gray rectangular area in the figure) disappeared in the ternary solid dispersions, which can indicate that Try is also involved in the formation of intermolecular hydrogen bonds in the solid dispersions and can be used as a proton donor. In addition, the absorption bands of the solid dispersion (yellow rectangular region in Fig. 16 are two distinctly separated peaks for both CBZ and Try samples at the same wavenumber range. The formation of the absorption bands also indicates the existence of intermolecular

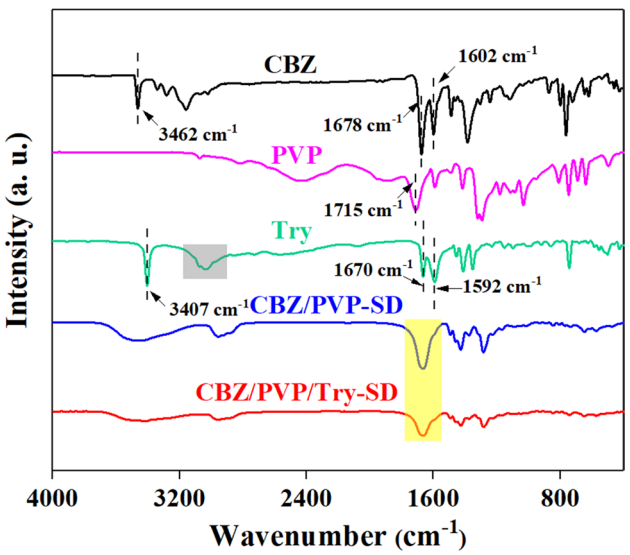

Fig. 16 FT-IR spectra of CBZ, PVP, Try, and two solid dispersions

interactions between CBZ and Try. This corresponds to the tendency to form Type A to Type B hydrogen bonds between CBZ and Try as discussed above in the molecular dynamic discussion.

UV–Vis Absorption Spectrum and Standard Curve of CBZ

In this part, the UV–Vis absorption spectra of five CBZ-ethanol solution samples with equal concentration gradients are shown in Fig. 17a. From the results, it can be obtained that the CBZ sample standard solution has the maximum absorption peak at the wavelength of 290 nm. And there is a standard linear relationship between absorbance and concentration in the concentration range of 2.8–25.2 μg/ml, as shown in Fig. 17b, with the fitted standard equation $r^2 = 0.9998$. This indicates that the subsequent dissolution assay of solid dispersions can be performed at this wavelength for absorbance determination and quantification of CBZ concentration.

Dissolution Test

According to the dissolution test described in the "Dissolution Test" section, the dissolution curves of CBZ, CBZ/PVP-SD, and CBZ/PVP/Try-SD can be obtained, and the dissolution curves are shown in Fig. 18. In Fig. 18, the *[CBZ]* refers to the cumulative concentration of CBZ. From the results, the dissolution plateaus of the three-part samples in the range of 0–180 min were in the order of CBZ/PVP/Try-SD > CBZ/PVP-SD > CBZ. On the one hand, the pure drug release rate was slow and did not reach 50% within 40 min, which is the defective for oral drug delivery. On the other hand, the dissolution plateau of CBZ/PVP/Try-SD was about 21% higher than that of CBZ/PVP-SD. The dissolution performance of ternary solid dispersions containing Try solid dispersion was also higher than that of solid binary dispersions, which revealed the performance advantage of the addition of the third component of organic small molecule excipient. This is consistent with the predictions of simulation parameters such as mean square displacement (*MSD*), binding interaction energy ($E_{binding}$), and hydrogen bonding concentrations (C_{HBs}).

Conclusion

In this study, the third component regulating CBZ/PVP solid dispersions was identified by multi-scale simulations based on miscibility and intermolecular hydrogen bonding. At the same time, the microscopic formation mechanism of the CBZ/PVP/Try ternary solid dispersion was quantified, and the corresponding solid dispersions were prepared to confirm the conjecture. The main contributions are as follows:

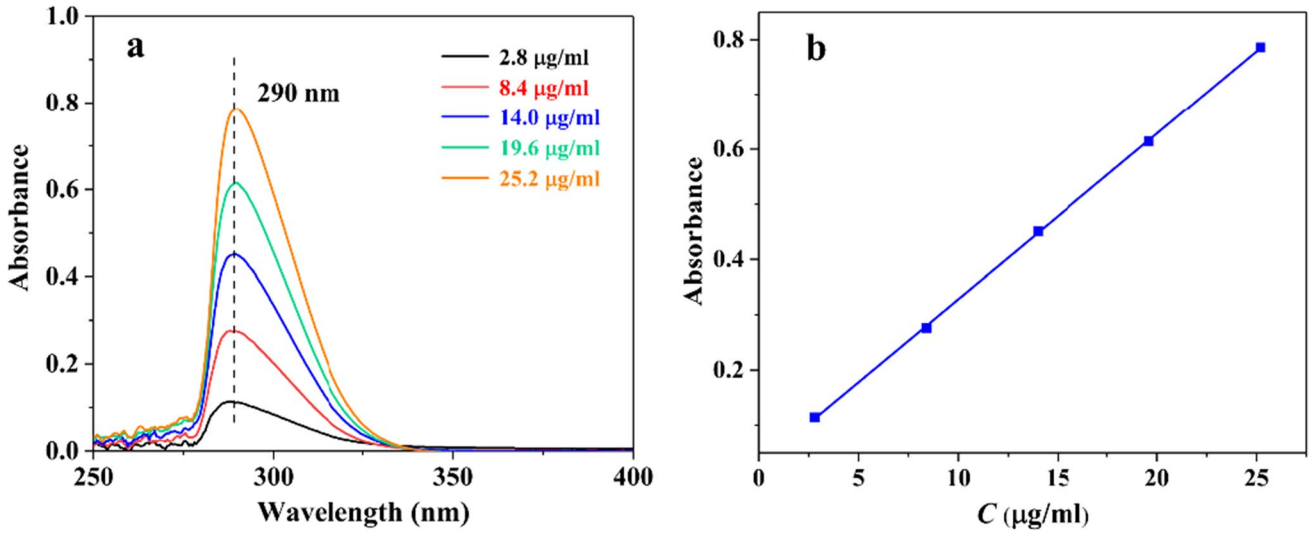

Fig. 17 **a** UV–Vis spectra and **b** standard curve of CBZ-anhydrous ethanol

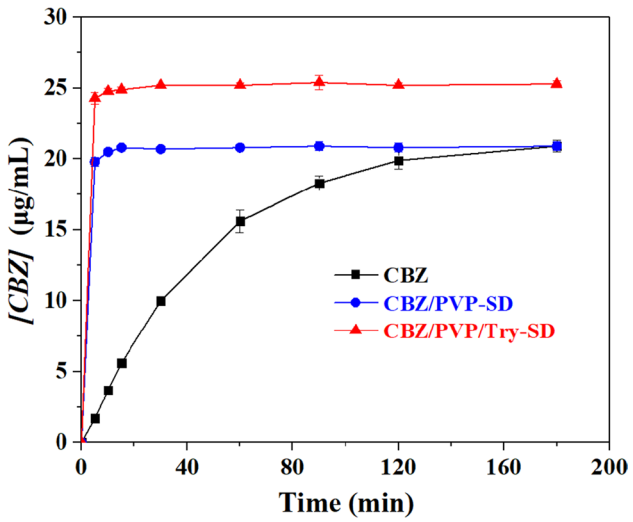

Fig. 18 Dissolution curves of CBZ drug and with two solid dispersion samples

(1) Based on the miscibility criteria and hydrogen bond strength analysis, from 13 organic small molecule candidate compounds, excellent amino acid (Try) was selected according to solubility parameters (δ), conjugated dimer conformation, hydrogen bond dissociation Gibbs free energy (ΔG), and dissociation equilibrium constant ($\ln K^{\theta}$).

(2) The binary system of CBZ/PVP was compared with the ternary system of CBZ/PVP/Try by means of molecular dynamics simulations. Analyzing the parameters of mean square displacement (*MSD*), diffusion coefficient (D), binding energy (E_{binding}), and concentration of hydrogen bonds (C_{HBs}), it was found that the drug mobility resistance, interactions, and hydrogen bonding content of the ternary system of CBZ/PVP/Try were higher than that of the binary system of CBZ/PVP. This analysis theoretically explains the mechanism of the solubility enhancement compared with the ternary system.

(3) The corresponding binary and ternary solid dispersions were prepared. The DSC, XRD, and SEM experimental results confirmed that the two solid dispersions achieved amorphous transformation compared to CBZ. FT-IR results showed that Try was involved in hydrogen bond formation in the solid dispersion. The solubility experimental results of drug release proved that the cumulative solubility of the ternary solid dispersion CBZ/PVP/Try-SD was about 21% higher than that of CBZ/PVP-SD.

In sum, this study may provide a new way for the design of drug modification and solid dispersion system, which has some theoretical guidance.

Author Contribution SZ: investigation, methodology, data curation, formal analysis, and writing—original draft.
HW: investigation and software.
XZ: supervision, methodology, and investigation.
HX: supervision, methodology conceptualization, and writing—review and editing.
SW: conceptualization, methodology, validation, and writing—review and editing.

Funding The authors gratefully acknowledge financial support from the original exploration project funded by National Science Foundation of China (Grant No. 52250357) and Fundamental Research Funds for the Central Universities (Grant No. 3332022038).

Data Availability The data that support the findings of this study are available from the corresponding author, upon reasonable request.

Declarations

Conflict of Interest The authors declare no competing interests.

References

1. Ting JM, Porter WW III, Mecca JM, Bates FS, Reineke TM. Advances in polymer design for enhancing oral drug solubility and delivery. Bioconjugate Chem. 2018;29(4):939–52.
2. Shi Q, Moinuddin SM, Cai T. Advances in coamorphous drug delivery systems. Acta Pharmaceutica Sinica B. 2019;9(1):19–35.
3. Qian F, Huang J, Hussain MA. Drug-polymer solubility and miscibility: stability consideration and practical challenges in amorphous solid dispersion development. J Pharm Sci. 2010;99(7):2941–7.
4. Singh L, Kaur L, Singh G, Dhawan RK, Kaur M, Kaur N, et al. Determination of alteration in micromeritic properties of a solid dispersion: Brunauer-Emmett-Teller based adsorption and other structured approaches. AAPS PharmSciTech. 2022;23(6):209.
5. Jermain SV, Brough C, Williams RO. Amorphous solid dispersions and nanocrystal technologies for poorly water-soluble drug delivery – an update. Int J Pharm. 2018;535(1):379–92.
6. Kong Y, Wang W, Wang C, Li L, Peng D, Tian B. Supersaturation and phase behavior during dissolution of amorphous solid dispersions. Int J Pharm. 2023;631: 122524.
7. Li J, Wang Y, Yu D. Effects of additives on the physical stability and dissolution of polymeric amorphous solid dispersions: a review. AAPS PharmSciTech. 2023;24(7):175.
8. Huang Y, Dai W-G. Fundamental aspects of solid dispersion technology for poorly soluble drugs. Acta Pharmaceutica Sinica B. 2014;4(1):18–25.
9. Wegiel LA, Zhao YH, Mauer LJ, Edgar KJ, Taylor LS. Curcumin amorphous solid dispersions: the influence of intra and intermolecular bonding on physical stability. Pharm Dev Technol. 2014;19(8):976–86.
10. Mureşan-Pop M, Pop MM, Borodi G, Todea M, Nagy-Simon T, Simon S. Solid dispersions of Myricetin with enhanced solubility: formulation, characterization and crystal structure of stability-impeding Myricetin monohydrate crystals. J Mol Struct. 2017;1141:607–14.
11. Hawkins BA, Du JJ, Lai F, Stanton SA, Williams PA, Groundwater PW, et al. An experimental and theoretical charge density study of theophylline and malonic acid cocrystallization. RSC Adv. 2022;12(25):15670–84.
12. Widanapathirana L, Tale S, Reineke TM. Dissolution and solubility enhancement of the highly lipophilic drug phenytoin via interaction with poly(N-isopropylacrylamide-co-vinylpyrrolidone) excipients. Mol Pharm. 2015;12(7):2537–43.
13. Ozaki S, Kushida I, Yamashita T, Hasebe T, Shirai O, Kano K. Inhibition of crystal nucleation and growth by water-soluble polymers and its impact on the supersaturation profiles of amorphous drugs. J Pharm Sci. 2013;102(7):2273–81.
14. Janssens S, Van den Mooter G. Review: physical chemistry of solid dispersions. J Pharm Pharmacol. 2010;61(12):1571–86.
15. Alshehri S, Imam SS, Altamimi MA, Hussain A, Shakeel F, Elzayat E, et al. Enhanced dissolution of luteolin by solid dispersion prepared by different methods: physicochemical characterization and antioxidant activity. ACS Omega. 2020;5(12):6461–71.
16. Xiong X, Zhang M, Hou Q, Tang P, Suo Z, Zhu Y, et al. Solid dispersions of telaprevir with improved solubility prepared by co-milling: formulation, physicochemical characterization, and cytotoxicity evaluation. Mater Sci Eng, C. 2019;105: 110012.
17. Zhang S, Wang T, Xue J, Xu H, Wu S. Hydrogen bonding principle-based molecular design of a polymer excipient and impacts on hydrophobic drug properties: molecular simulation and experiment. Biomacromol. 2023;24(4):1675–88.
18. Alves LDS, de La Roca Soares MF, de Albuquerque CT, da Silva ÉR, Vieira ACC, Fontes DAF, et al. Solid dispersion of efavirenz in PVP K-30 by conventional solvent and kneading methods. Carbohydr Polym. 2014;104:166–74.
19. Sathisaran I, Dalvi SV. Investigating cocrystallization of carbamazepine with structurally compatible coformers: new cocrystal and eutectic phases with enhanced dissolution. AAPS PharmSciTech. 2021;22(1):29.
20 Yarlagadda DL, Sai Krishna Anand V, Nair AR, NavyaSree KS, Dengale SJ, Bhat K. Considerations for the selection of co-formers in the preparation of co-amorphous formulations. Int J Pharm. 2021;602:120649.
21. Gao Y, Liao J, Qi X, Zhang J. Coamorphous repaglinide–saccharin with enhanced dissolution. Int J Pharm. 2013;450(1):290–5.
22. Wu W, Ueda H, Löbmann K, Rades T, Grohganz H. Organic acids as co-formers for co-amorphous systems – influence of variation in molar ratio on the physicochemical properties of the co-amorphous systems. Eur J Pharm Biopharm. 2018;131:25–32.
23. Fung MH, Suryanarayanan R. Effect of organic acids on molecular mobility, physical stability, and dissolution of ternary ketoconazole spray-dried dispersions. Mol Pharm. 2019;16(1):41–8.
24. Liu J, Rades T, Grohganz H. Determination of the optimal molar ratio in amino acid-based coamorphous systems. Mol Pharm. 2020;17(4):1335–42.
25. Karagianni A, Kachrimanis K, Nikolakakis I. Co-amorphous solid dispersions for solubility and absorption improvement of drugs: composition, preparation, characterization and formulations for oral delivery. Pharmaceutics. 2018;10(3):98.
26. Martínez LM, Videa M, López Silva T, Castro S, Caballero A, Lara-Díaz VJ, et al. Two-phase amorphous-amorphous solid drug dispersion with enhanced stability, solubility and bioavailability resulting from ultrasonic dispersion of an immiscible system. Eur J Pharm Biopharm. 2017;119:243–52.
27. Veith H, Wiechert F, Luebbert C, Sadowski G. Combining crystalline and polymeric excipients in API solid dispersions – opportunity or risk? Eur J Pharm Biopharm. 2021;158:323–35.
28. Zhang S, Zhang X, Meng J, Lu L, Du S, Xu H, et al. Study on the effect of polymer excipients on the dispersibility, interaction, solubility, and scavenging reactive oxygen species of myricetin solid dispersion: experiment and molecular simulation. ACS Omega. 2022;7(1):1514–26.
29. Schittny A, Philipp-Bauer S, Detampel P, Huwyler J, Puchkov M. Mechanistic insights into effect of surfactants on oral bioavailability of amorphous solid dispersions. J Control Release. 2020;320:214–25.
30. Pajula K, Taskinen M, Lehto V-P, Ketolainen J, Korhonen O. Predicting the formation and stability of amorphous small molecule binary mixtures from computationally determined Flory–Huggins interaction parameter and phase diagram. Mol Pharm. 2010;7(3):795–804.
31. Gupta J, Nunes C, Vyas S, Jonnalagadda S. Prediction of solubility parameters and miscibility of pharmaceutical compounds by molecular dynamics simulations. J Phys Chem B. 2011;115(9):2014–23.
32. Gupta KM, Chin X, Kanaujia P. Molecular interactions between APIs and enteric polymeric excipients in solid dispersion: insights from molecular simulations and experiments. Pharmaceutics. 2023;15(4):1164.

33. Koromili M, Kapourani A, Barmpalexis P. Preparation and evaluation of amorphous solid dispersions for enhancing Luteolin's solubility in simulated saliva. Polymers. 2023;15(1):169.
34. Chakravarty P, Lubach JW, Hau J, Nagapudi K. A rational approach towards development of amorphous solid dispersions: experimental and computational techniques. Int J Pharm. 2017;519(1):44–57.
35. Li B, Wang Y, Feng Y, Yuan D, Xu R, Jiang C, et al. Design and molecular insights of drug-active metabolite based co-amorphous formulation: a case study of toltrazuril-ponazuril co-amorphous. Int J Pharm. 2022;615: 121475.
36. Qian F, Huang J, Hussain MA. Drug–polymer solubility and miscibility: stability consideration and practical challenges in amorphous solid dispersion development. J Pharm Sci. 2010;99(7):2941–7.
37. Chiș I-A, Andrei V, Muntean A, Moldovan M, Mesaroș AȘ, Dudescu MC, et al. Salivary biomarkers of anti-epileptic drugs: a narrative review. Diagnostics. 2023;13(11):1962.
38. Hong G-Y, Hu X, Wang F, Li L-M. An approach to reduce the computational effort in accurate DFT calculations. Chem Phys. 2003;290(2):163–70.
39. Fischer M, Evers FO, Formalik F, Olejniczak A. Benchmarking DFT-GGA calculations for the structure optimisation of neutral-framework zeotypes. Theoret Chem Acc. 2016;135(12):257.
40. Delley B. Ground-state enthalpies: evaluation of electronic structure approaches with emphasis on the density functional method. J Phys Chem A. 2006;110(50):13632–9.
41. Zhu J, Zhao X, Liu L, Yang R, Song M, Wu S. Thermodynamic analyses of the hydrogen bond dissociation reaction and their effects on damping and compatibility capacities of polar small molecule/nitrile-butadiene rubber systems: molecular simulation and experimental study. Polymer. 2018;155:152–67.
42. Hu C, You G, Liu J, Du S, Zhao X, Wu S. Study on the mechanisms of the lubricating oil antioxidants: experimental and molecular simulation. J Mol Liq. 2021;324: 115099.
43. Ueda H, Wu W, Löbmann K, Grohganz H, Müllertz A, Rades T. Application of a salt coformer in a co-amorphous drug system dramatically enhances the glass transition temperature: a case study of the ternary system carbamazepine, citric acid, and l-arginine. Mol Pharm. 2018;15(5):2036–44.
44. Wu W, Wang Y, Löbmann K, Grohganz H, Rades T. Transformations between co-amorphous and co-crystal systems and their influence on the formation and physical stability of co-amorphous systems. Mol Pharm. 2019;16(3):1294–304.
45. Liu J, Zhang S, Zhao X, Lu Y, Song M, Wu S. Molecular simulation and experimental study on the inclusion of rutin with β-cyclodextrin and its derivative. J Mol Struct. 2022;1254: 132359.
46. Luo K, Ye X, Zhang H, Liu J, Luo Y, Zhu J, et al. Vulcanization and antioxidation effects of accelerator modified antioxidant in styrene-butadiene rubber: experimental and computational studies. Polym Degrad Stab. 2020;177: 109181.
47 Minch MJ. An introduction to hydrogen bonding (Jeffrey, George A.). J Chem Educ. 1999;76(6):759.
48. Asnin LD, Stepanova MV. Van't Hoff analysis in chiral chromatography. Journal of Separation Science. 2018;41(6):1319–37.
49. van Zon R, Schofield J. Constructing smooth potentials of mean force, radial distribution functions, and probability densities from sampled data. J Chem Phys. 2010;132(15): 154110.
50. Xu K, Zhang F, Zhang X, Hu Q, Wu H, Guo S. Molecular insights into hydrogen bonds in polyurethane/hindered phenol hybrids: evolution and relationship with damping properties. J Mater Chem A. 2014;2(22):8545–56.
51. Yu D, Li J, Wang H, Pan H, Li T, Bu T, et al. Role of polymers in the physical and chemical stability of amorphous solid dispersion: a case study of carbamazepine. Eur J Pharm Sci. 2022;169:106086.
52. Červinka C, Fulem M. Structure and glass transition temperature of amorphous dispersions of model pharmaceuticals with nucleobases from molecular dynamics. Pharmaceutics. 2021;13(8):1253.
53. Holzapfel K, Rades T, Leopold CS. Co-amorphous systems consisting of indomethacin and the chiral co-former tryptophan: solid-state properties and molecular mobilities. Int J Pharm. 2023;636:122840.

Publisher's Note Springer Nature remains neutral with regard to jurisdictional claims in published maps and institutional affiliations.

Springer Nature or its licensor (e.g. a society or other partner) holds exclusive rights to this article under a publishing agreement with the author(s) or other rightsholder(s); author self-archiving of the accepted manuscript version of this article is solely governed by the terms of such publishing agreement and applicable law.